SANDIA REPORT
SAND2008-6516
Unlimited Release
Printed October 2008

Nanoparticle Flow, Ordering and Self-Assembly

Gary S. Grest, W. Michael Brown, Jeremy B. Lechman, Matt K. Petersen, Steven J. Plimpton, P. Randall Schunk

Prepared by
Sandia National Laboratories
Albuquerque, New Mexico 87185 and Livermore, California 94550

Sandia is a multiprogram laboratory operated by Sandia Corporation,
a Lockheed Martin Company, for the United States Department of Energy's
National Nuclear Security Administration under Contract DE-AC04-94AL85000.

Issued by Sandia National Laboratories, operated for the United States Department of Energy by Sandia Corporation.

Available to DOE and DOE contractors from
U.S. Department of Energy
Office of Scientific and Technical Information
P.O. Box 62
Oak Ridge, TN 37831

Telephone: (865) 576-8401
Facsimile: (865) 576-5728
E-Mail: reports@adonis.osti.gov
Online ordering: http://www.osti.gov/bridge

Available to the public from
U.S. Department of Commerce
National Technical Information Service
5285 Port Royal Rd.
Springfield, VA 22161

Telephone: (800) 553-6847
Facsimile: (703) 605-6900
E-Mail: orders@ntis.fedworld.gov
Online order: http://www.ntis.gov/help/ordermethods.asp?loc=7-4-0#online

SAND2008-6516
Unlimited Release
Printed October 2008

Nanoparticle Flow, Ordering and Self-Assembly

Gary S. Grest, W. Michael Brown, Jeremy B. Lechman, Matt K. Petersen, Steven J. Plimpton, P. Randall Schunk
Sandia National Laboratories
P.O. Box 5800
Albuquerque, New Mexico 87185

Pieter J. in 't Veld
Polymer Research BSF SE, 67056 Ludwigshafen, Germany

Abstract

Nanoparticles are now more than ever being used to tailor materials function and performance in differentiating technologies because of their profound effect on thermo-physical, mechanical and optical properties. The most feasible way to disperse particles in a bulk material or control their packing at a substrate is through fluidization in a carrier, followed by solidification through solvent evaporation/drying/curing/sintering. Unfortunately processing particles as concentrated, fluidized suspensions into useful products remains an art largely because the effect of particle shape and volume fraction on fluidic properties and suspension stability remains unexplored in a regime where particle-particle interaction mechanics is prevalent. To achieve a stronger scientific understanding of the factors that control nanoparticle dispersion and rheology we have developed a multiscale modeling approach to bridge scales between atomistic and molecular-level forces active in dense nanoparticle suspensions. At the largest length scale, two "coarse-grained" numerical techniques have been developed and implemented to provide for high-fidelity numerical simulations of the rheological response and dispersion characteristics typical in a processing flow. The first is a coupled Navier-Stokes/discrete element method in which the background solvent is treated by finite element methods. The second is a particle based method known as stochastic rotational dynamics. These two methods provide a new capability representing a "bridge" between the molecular scale and the engineering scale, allowing the study of fluid-nanoparticle systems over a wide range of length and timescales as well as particle concentrations. To validate these new methodologies, multi-million atoms simulations explicitly including the solvent have been carried out. These simulations have been vital in establishing the necessary "subgrid" models for accurate prediction at a larger scale and refining the two coarse-grained methodologies.

CONTENTS

INTRODUCTION

Growing advancement of nanoparticle fabrication techniques and analytical instrumentation has renewed the colloidal chemistry field and its application to nanoparticle composite manufacturing. Nanoparticles are particles on the size of one to hundreds of nanometers, which, due to their small size, are mass efficient for modifying bulk and surface properties. They can now be made from a wide range of materials with unprecedented control of size and shape. There is also a rich set of possible nanoparticle coatings, particularly using the biochemistry of peptides and DNA, yielding new surface interactions. A distinct advantage of nanoparticles is that highly efficient and inexpensive polymer processing methods can be used to fabricate significant quantities of the composite material. Composites consisting of dispersed or ordered nanoparticle building blocks can be tailored to exhibit materials properties that have been unachievable with conventional materials, including increased strength and toughness of films and fibers to enhanced optical characteristics of coatings.

The most feasible way to disperse particles in a bulk material or control their packing at a substrate is through fluidization in a carrier that can be processed with well-known techniques such as spin, drip and spray coating, fiber drawing, casting followed by solidification through solvent evaporation/drying/curing/sintering [1]. Unfortunately processing nanoparticles as concentrated, fluidized suspensions is a primary challenge and remains an art largely because of the extraordinary effect of particle shape and volume fraction on fluidic (rheological) properties. A second challenge is to create stable dispersions that can be processed into films, fibers, and other bulk structures. If the nanoparticles stick together and flocculate they cannot be processed. A schematic of the various interaction forces that are relevant on the nanoscale is shown in Figure 1. Clearly scientific understanding at multiple length scales, from atomistic to continuum, is crucial to surmounting these challenges in designing and manufacturing nanocomposite materials.

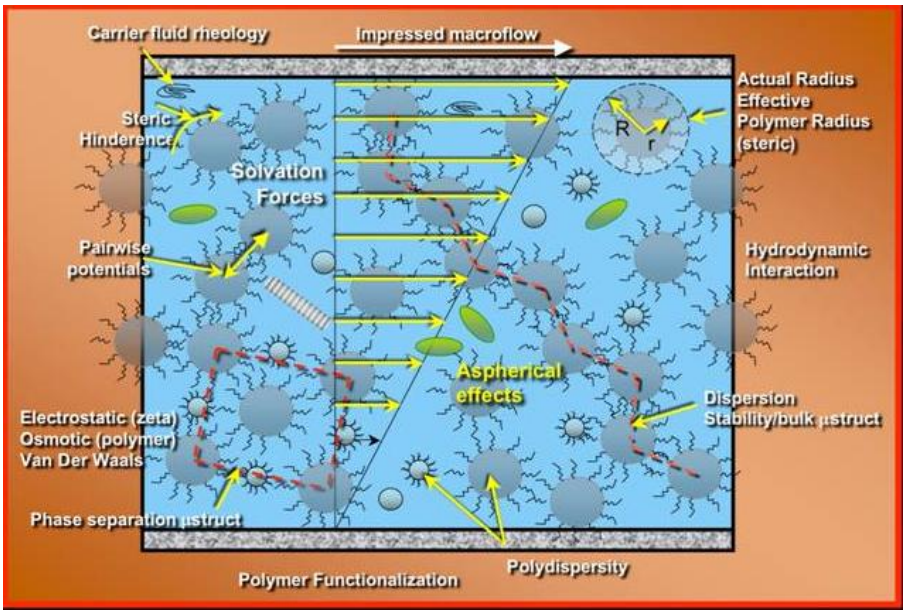

FIGURE 1: Illustration of the rich physical phenomena that control nanoparticle stability and rheology.

To achieve a stronger scientific understanding of the factors that control nanoparticle dispersion and rheology we have developed a multiscale modeling approach to bridge scales between atomistic and molecular-level forces active in dense nanoparticle suspensions. As the particle size decreases to the nanometer scale a number of complications not present in modeling large micron sized colloidal particles arise. One is that the natural length scale of the background solvent which for colloidal suspensions is much smaller than the colloid is now comparable to the size of the nanoparticles. Another is that the form of the effective potential between nanoparticles is not known. This is largely due to the fact that short chain surfactants which are often added to the particle surface to prevent flocculation are not comparable in size to the nanoparticle itself. To overcome these complications we have developed a multi-prong numerical approach. At the largest length scale, two "coarse-grained" numerical techniques have been developed and implemented to provide for high-fidelity numerical simulations of the rheological response and dispersion characteristics typical in a processing flow. The first is a coupled Navier-Stokes/discrete element method (NS/DEM) in which the background solvent is treated by finite element methods. The second is a particle based method known as stochastic rotational dynamics (SRD) [2-4]. These two methods provide a new capability representing a "bridge" between the molecular scale and the engineering scale, allowing the study of fluid-nanoparticle systems over a wide range of length and timescales as well as particle concentrations. To validate these new methodologies, particularly in regard to testing the minimum size of a nanoparticle and bulk concentration of particles at which the continuum fluid-solver approach is valid, multi-million atoms simulations explicitly including the solvent have been carried out. These simulations have been vital in establishing the necessary "subgrid" models for accurate prediction at a larger scale and refining the NS/DEM and SRD methodologies. To determine the forces between the nanoparticles which are required input to these approaches, molecular dynamics simulations with full atomistic detail are being used. The results of this aspect of the work will be presented in a later report. In this report we present high-level descriptions of every aspect of this project, and conclude with a clear statement of new capabilities in modeling and simulation, as well as a discussion of future opportunities.

Coarse-grained Solvent Methods

When speaking of nano-colloid suspension rheology what we seek is a relationship between stress and strain-rate. In general we seek transport coefficients and their functional dependence upon system parameters such as shear rate or colloid volume fraction. In particular, we seek to be predictive for a range of colloid material, polymer functionalization, charge, and solvents with regard to mass transport (diffusion coefficient) and momentum transport (viscosity). A schematic of the possible physical phenomena in the systems to be modeled are pictured in Fig. 1. Note that solvent hydrodynamics (colloid-colloid and macroscopically induced flow), solvent removal and a plethora of colloid-colloid/colloid-solvent interactions must all be accounted for. Resolving these predictively is a challenge for any single method; hence we have approached this problem from several directions attempting to develop a set of tools and the understanding of the conditions under which each is applicable and the trade-offs inherent in the choice of one method vis-à-vis the others.

Before the details of the methods investigated are presented it is well to consider the computational options and requirements that the model system places on each method. Consider Fig. 1 again. Let's say that we are interested in the viscosity of a suspension of spherical nano-colloids of size 100 nm at volume fraction 50% in some general solvent (perhaps water). As a general rule, it is known that, in order to obtain good statistics and avoid finite size effects, several hundred to one thousand spheres are required to determine the viscosity in a numerical simulation. Given this, the simulation domain to be simulated is on the order of μm^3. Suppose also that we want to shear the system at 100 sec^{-1}. Again, in order to obtain good data, a total strain of about 10 box units is a good rule-of-thumb. This requires a simulation of about 0.1 μsec of real time. With these parameters in mind, let us consider the potential numerical methods to solve this problem.

First, it should be noted that an explicit, atomistic representation of the problem will be limited by the smallest length and timescales in the system (i.e., the individual atoms of the solvent/colloid). Even with the cpu resources available at Sandia these types of calculations are limited to system sizes on the order of tens to hundreds of nanometers and total real time on the order of 10 to 100 nano-seconds. Although these types of calculations are vital for discovering the effects of the molecular details of a particular system they are by nature prohibitive in most cases for the rheological information sought.

The way to get around the severity of this limitation is to "coarse-grain", i.e., reduce the number of degrees of freedom in the problem by averaging over the "fast" ones. This is possible assuming that the timescales are sufficiently separated. Both the colloids and the solvent are potential candidates for coarse-graining in order to make the problem computationally tractable. In section III, a model coarse-grained colloid is discussed and simulated in an explicit LJ solvent. This is made possible due to advances in LAMMPS [5] numerical algorithm and data structure to handle disparate sizes efficiently [6]. In this way, explicit atom solvent simulations are made tractable. What is required is knowledge of the coarse-grained or "effective" potential of the colloid-colloid and colloid-solvent interactions. This information is required for all simulation methods and can be obtained through a coupled theoretical/simulation and experimental (e.g., laser-tweezers, IFM) program for a particle suspension formulation.

A second issue to note is that the solvent itself is also a candidate for coarse-graining. Additionally, further approximations can be made so that the simulation can be made more computationally efficient; albeit at a price. As Irving and Kirkwood [7] have shown, the Navier-Stokes equations are derivable from ensemble averages of conservation of microscopic momentum. Thus, simply coupling the discrete colloids to a continuum Navier-Stokes solver is one approach to relaxing the restrictions of atomistic timescales in the solvent while retaining the main effect of hydrodynamic interactions. The cost is the loss of certain atomistic details that it is hoped can be accounted for in effective potentials and boundary conditions. As noted above, additional approximations can be made, which are often times inherent in particle-based coarse-grained solvent methods for modeling hydrodynamics. This involves what has been called "collapsing" or "telescoping" the timescales [3]. In the actual system there are multiple timescales that can be separated by many orders of magnitudes. Collapsing the timescales involves changing the timescales in the problem so that the separation between them is reduced, perhaps on one order of magnitude as opposed to three or four. This results in certain computational efficiencies at the cost of a loss of one-to-one correspondence between the model

and real systems. What is hoped for is that the physics of the problem are not too sensitive to these changes and dynamic similarity can be achieved. However, to be predictive with these methods requires rigorous validation of the approximations that went into the models. Hence, user control over the "telescoping" is required, which can be accomplished thorough implanting a Navier-Stokes solver such as FEM.

In summary, the quest for modeling and simulation tools which meet the needs of this research and development project, no single simulation method enables predictive nanoparticle suspension dynamics and rheology across the breadth of required features. The most critical requirements are as follows: (1) computational efficiency and scalability, (2) solvent fluid mechanics accuracy and generality (e.g., non-Newtonian fluids), (3) ability to couple fluids and the discrete particle nature of nanoparticle interactions and associated dynamics, (4) spherical and generally aspherical particles, and (5) user-friendly for real-system simulations. As described in Section II.2, Stochastic Rotation Dynamics (SRD) meets requirements (1), (3), and (4) as well as any other method. To meet requirements (2) and (5), we also advanced a generalized Navier-Stokes/Discrete-element capability which is the subject of the next section.

Coupled Finite Element – Discrete Element Methods

Recall that our goal is to simulate larger length scales and longer times. To achieve this, we need to relax the dependence on the smallest length and time scales while capturing the dominant effects of these. In many cases it is assumed that the dominant effect of the solvent which can not be easily captured by pair-wise, conservative, coarse-grained effective potentials is the effect of hydrodynamic interactions between the colloids since they are many-body, long-range, dissipative interactions. Thus, the "coarse-graining" suggested here is to simply couple discrete colloids to a Navier-Stokes solver. In this way only the timescales associated with the macroscopic properties of the bulk fluid, colloids and flow field are relevant. Additional approximations, such as are inherent in particle-based coarse-graining methods (e.g., dissipative particle dynamics (DPD) [8-12], SRD [2-4]), which reduce the separation between various timescales can also be applied. For instance, by increasing the compressibility of the solvent (reducing the sound speed) one can reduce the sound travel time, or similarly the momentum diffusion time through the solvent can be adjusted through the kinematic viscosity. Implementing a Navier-Stokes solve thus gives a way of validating that the relevant physics have not been compromised by an assumption of dynamic similarity between the model and real systems.

We use a Finite Element Method for solving the Navier-Stokes equations in this work and seek to couple it with LAMMPS as a discrete particle dynamics solver. LAMMPS, therefore, handles all the details regarding the coarse-grained colloid-colloid interactions as mediated by the solvent. Using a FEM approach for hydrodynamics will give us an accurate, robust and general capability. However, in this work we make certain simplifying assumptions to allow us to begin development of coupled discrete-continuum approach. Specifically, we assume the solvent is a Newtonian, incompressible fluid with constant density. In this case the Navier-Stokes equations take the form

$$\frac{\partial \mathbf{u}}{\partial t} + \mathbf{u} \cdot \nabla \mathbf{u} = -\nabla p + \nu \nabla^2 \mathbf{u}$$

$$\nabla \cdot \mathbf{u} = 0$$

plus boundary and initial conditions.

Traditional approaches to solving for both the pressure and the velocity at the same time in a "mixed" FEM formulation of the problem can be very computationally intensive due to the poor conditioning of the matrix equations. In order to alleviate this difficulty we developed and implemented a fractional stepping or projection-type algorithm which solves for the velocity and pressure separately through use of the fact that the incompressibility constraint (divergence of the velocity field equal to zero) can be rewritten as a so-called Pressure Poisson Equation. This allows for a decoupling of the pressure and velocity solves. The algorithm we use consists of four steps. In time discretized form these are:

$$1)\ \frac{\mathbf{u}^* - \mathbf{u}^n}{\Delta t} = (\mathbf{u} \cdot \nabla \mathbf{u})^n + \nabla p^{n-1/2} - \frac{\nu}{2} \nabla (\mathbf{u}^* + \mathbf{u}^n)$$

$$2)\ \nabla^2 \phi^{n+1} = \nabla \cdot \mathbf{u}^*$$

$$3)\ \mathbf{u}^{n+1} = \mathbf{u}^* - \Delta t \nabla \phi^{n+1}$$

$$4)\ p^{n+1/2} = p^{n-1/2} + \phi^{n+1} - \frac{\nu}{2} \nabla \cdot \mathbf{u}^*$$

where we have introduced an intermediate, non-solenoidal velocity field, u* and an intermediate pressure field, ϕ. Steps 1-4 also need appropriate boundary and initial conditions, which for the most part are standard. However, the boundary condition on Step 2 does merit further comment. First, we note that for our implementation ϕ^{n+1} should be interpreted as a pressure increment ($\phi^{n+1} = p^{n+1/2} - p^{n-1/2}$) so that as Steps 1-4 are iterated, u* converges to u^{n+1}, the "correct" solenoidal velocity field. Hence, ϕ^{n+1} must go to zero as the divergence of u* goes to zero (cf. Step 4). This means that boundary conditions of Step 2 must insure the trivial solution when u* is solenoidal.

Previous implementations of fractional stepping-type algorithms have found very weak stability for second-order schemes where the pressure field depends on the time step [12] and have been hampered by issues surrounding correct numerical boundary conditions have lead to poor accuracy in the pressure field [13]. For our implementation we found no dependence of the results on the time step for the pressure gradient and velocity profile in a simple Poiseuille flow, the drag force on a fixed sphere at moderate Reynolds number, as well as for the drag force on a sphere in a simple cubic array of particles at zero Reynolds number. For the results of the latter case see Fig. 2 where we compare both the drag force calculated via FEM by fully-coupled pressure-velocity and pressure projection schemes to the very accurate numerical results of Ladd [14]. Results of a single particle with periodic boundary conditions as well as 3 by 3 by 3 and 5

by 5 by 5 arrays of spheres are shown to compare will with Ladd's results. In Fig. 3 results for varying the grid size of the 5 x 5 x 5 cubic array of spheres at one packing fraction (27%) are shown. Second order convergence in space can be clearly seen. These typical results are the most relevant for the current application in that LAMMPS only needs to know the total hydrodynamic force and torque on a colloid. These and similar results show that this algorithm can provide accurate values for these quantities.

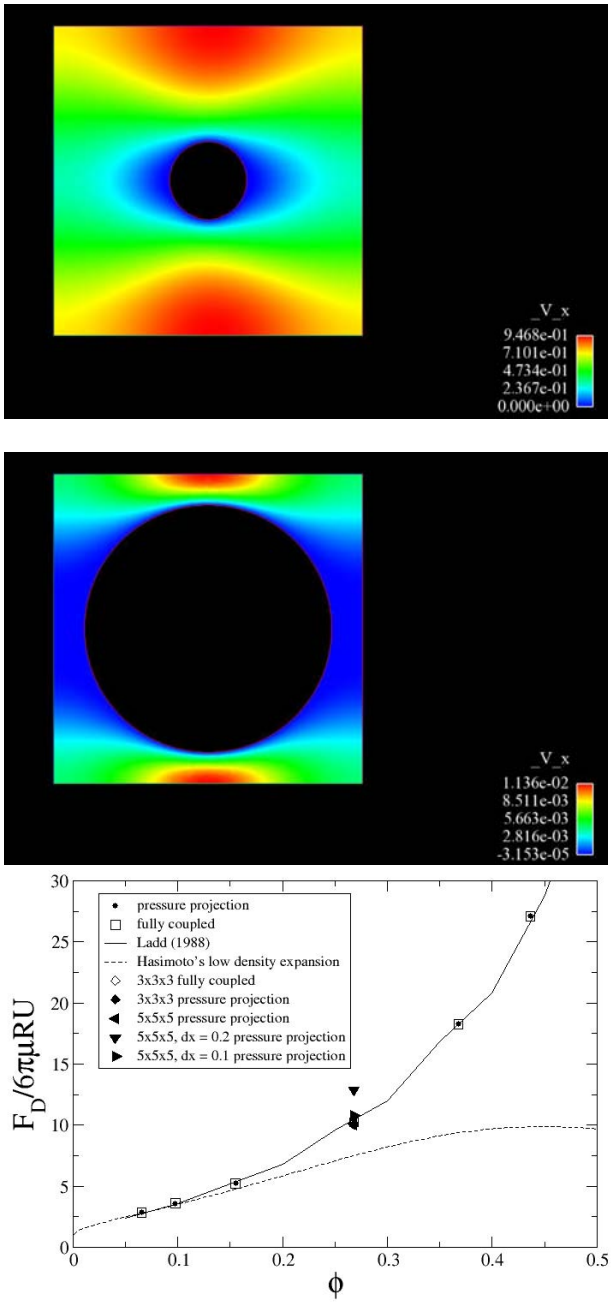

FIGURE 2: : Comparison of various numerical solutions for the average drag force on spheres of diameter 1.0 arranged in a square lattice at various volume fractions due to small Reynolds number flow through the lattice. Symmetry boundary conditions are employed for systems of 1 sphere, 3x3x3 spheres and 5x5x5 spheres. Also shown are cross-sections of the x-component of the flow field for a single sphere system.

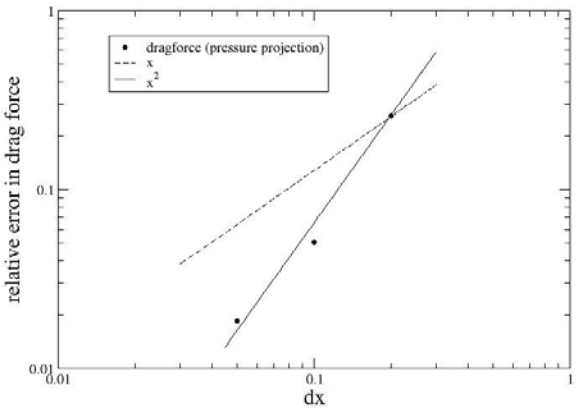

FIGURE 3: Error convergence of the average drag force on spheres of diameter 1.0 in a 5x5x5 square lattice at 27% volume fraction due to small Reynolds number flow through the lattice.

In Fig. 4 we show the computational efficiency of this scheme as compared with a direct-solve fully coupled u-p simulation. The figure shows the ratio of the cpu time to solve the problem on more than two processors to the time required to solve the problem on two processors. That is, we hold the total number of unknowns fixed and increase the number of processors and compare the runtime. These results are for a system with just over 1 million unknowns. It is estimated that we will routinely need to solve for approximately 10 million unknowns in order to simulate the systems described in Figure 1. Such a system would then be 10 times larger than the one used for Figure 4. As can be seen, the pressure projection scheme scales nearly ideally for more than about 64,000 unknowns per processor whereas the fully coupled approach can not be run on fewer than 16 processors. Hence, using the algorithm described here we can solve a given system on fewer processors while still taking advantage to parallel speed-up. It remains to be seen how the method scales as we increase the number of unknowns while holding the number of unknowns per processor constant.

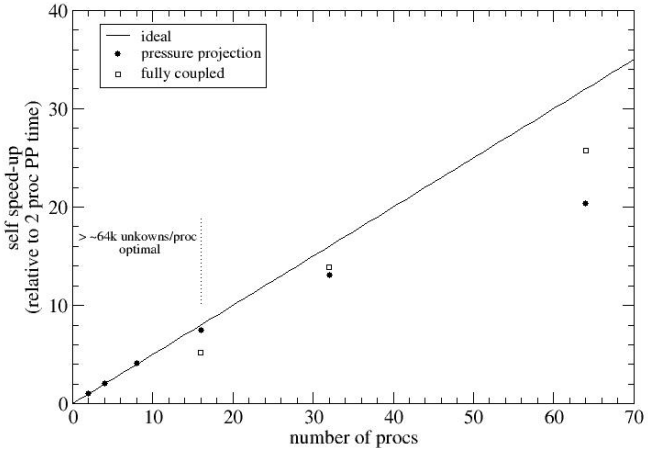

FIGURE 4: Performance results for system of 1,071,755 unknowns

In order to have a fully applicable FEM-based capability for predictive nano-colloid rheology modeling and simulation several tasks remain. Most crucial are having the ability to move particles through the domain with out remeshing. Currently, we are validating a novel one-level cut adaptively approach developed at Sandia called CDFEM. This allows particle to move through a uniform background mesh whose elements are cut by the particle surface and adapted to conform to their geometry. This approach has been shown to be accurate and efficient for simple systems and we are extending it application to nano-colloid rheology. In addition, we are developing stochastic terms to be added to the traditional Navier-Stokes terms to model thermal fluctuations in the fluid which drive Brownian motion. These are being developed and validated in an FEM formulation.

Stochastic Rotation Dynamics and Nano-Colloid Rheology

The SRD method fits into a broad category of "coarse-grained, particle-based solvent" methods for modeling hydrodynamics. The main advantage of these approaches is the computational expediency of discrete particle mechanics. These coarse-graining methods are further categorized based on interaction-type of the solvent particles. For instance, the Dissipative Particle Dynamics (DPD) method [8-11] combines classical molecular dynamics using conservative, soft-potentials for access to longer timescales with dissipative and random forces (i.e., a novel pair-wise momentum conserving thermostat) to accomplish full hydrodynamics of the solvent. Because of its similarity to classical molecular dynamics (MD), DPD methods are often available in MD codes like LAMMPS. Other particle-solvent approaches include the lattice-Boltzmann method (LB) [15], the vortex method, and direct simulation Monte Carlo (DSMC). Details of these methods and their limitations can be found in [3]. The SRD method is similar to LB and DPD methods, but accomplishes several improvements. Specifically, improvements have been realized in establishing a more firm statistical-mechanical basis, more-easily incorporating large-colloidal particles, and improving computational efficiency, cf. references [3] and [16].

In this project we advanced an SRD method in the classical MD code LAMMPS specifically aimed at coupled colloid-dynamics and fluid mechanics, viz. nanoparticle suspension dynamics. The SRD algorithm accounts for the hydrodynamics of the solvent and participates in the fluid-nanoparticle coupling, and an extended discrete element method (DEM) solver handles the colloid-colloid interactions and colloid dynamics. The coupled method has been implemented in LAMMPS. We built on previous work by Hecht *et al.*[2] and Padding and Louis [3] in this application area, with specific modifications and improvements in modeling shearing flows, the verification and validation of the method with respect to colloid diffusion and colloid-suspension rheology, and the computational data handling to make the method efficient and scalable on parallel architectures. With the exception of limited validation of colloid diffusion, these aspects were not specifically addressed by other research groups.

The concepts of SRD and associated algorithms are detailed in other papers (cf. Padding and Louis [3]). Those references can be consulted for details. In this report we will give a broad overview of our implementation.

SRD involves a large number N of particles (often referred hereafter as "SRDs", or "SRD-particles") endowed with mass but no inherent size. Particle positions are advanced through a Forward Euler-type streaming step over which no interactions occur. Hence for the i^{th} particle

$$\mathbf{x}_i(t+\Delta t) = \mathbf{x}_i(t) + \Delta t \mathbf{v}_i(t)$$

The fundamental length scale associated with SRD is brought in through so-called lattice bins into which the overall domain is tessellated. These bins are taken as uniform in size with primary dimension a_0. After the streaming step, the particles are subjected to a collision step, in which the velocity of each particle in a bin minus the bin-mass-average-velocity is rotated about a randomly-chosen axis over a fixed angle.

$$\mathbf{v}_i(t+\Delta t) = \bar{\mathbf{u}}_{bin}(t+\Delta t) + \Omega[\mathbf{v}_i(t) - \bar{\mathbf{u}}_{bin}(t+\Delta t)]$$

Where

$$\bar{\mathbf{u}}_{bin}(t+\Delta t) = (1/M)\sum_{i \in bin} \mathbf{v}_i(t)$$

is the average velocity of the particles in the bin, and Ω is a randomly chosen rotation matrix.

Malevanets and Kapral [4] have shown that this generates an equilibrium Maxwellian srd-particle velocity distribution and that it yields the correct hydrodynamic equations with an ideal-gas equation of state. It is noteworthy that each of the N srd-solvent particles represents much more than a solvent molecule and so care must be taken in specifying their mass, number density and mean-free path so as to attain the correct thermodynamic/kinematic quantities.

With respect to the colloid dynamics, or "big" particles, there are two modes of srd-collision which we have implemented: slip and no-slip. It remains a matter of research as to which mode represents a more accurate description for a given colloid and solvent; we have mainly used a no-slip stochastic collision process [3,17], in which an SRD-particle can impart linear and angular momentum to a nano-colloid. Note that Brownian forces on the colloids due to solvent thermal fluctuations are intrinsic to this method. Setting the SRD bath temperature is required, and, depending on the situation, thermostat or other considerations must be taken to help maintain the desired temperature since the SRD method is an NVE-like technique.

A more detailed discussion of the method is beyond the scope of this report. The other aforementioned sources, e.g. [2] and [3], along with references [18-20] provide further details. We will focus the discussion on the principles for setting the relevant model parameters. We will then provide some examples.

SRD simulation parameters consist of the lattice spacing a_0, the average number of fluid particles in a bin (or lattice cell), M, the SRD time step Δt_{srd}, the mass of the fluid (srd) particles m_f, and the rotation angle α. Since we want to resolve hydrodynamics on a scale smaller than a colloid

of radius R, we choose the lattice constant, or lattice spacing, as $a_0 = R/2$. In 3D this means that each spherical colloid particle will cover about 34 bins. Others have shown this to be near the upper limit for accurate resolution of the drag force on a sphere [14]. If the unit of length is chosen as the colloid diameter d, then $a_0 = 0.25$d. In this bin, at each SRD time step, the srd-particle velocities relative to the mean bin velocity are rotated by an angle $+\alpha$ or $-\alpha$ with probability 1/2 about randomly chosen axis, and the velocities of each particle are recomputed. It has been shown that $\alpha = \pi/2$ is optimal for fast relaxation to equilibrium [19]; we set this as a constant in our implementation. The particles are also allowed to collide with the colloids that intersect a bin.

For computational efficiency, a number of SRD particles per bin M between 3 and 6 is a good choice. Actually, this is not an explicit input in our implementation, but rather a result of setting a_0 and the total number of SRD particles at initialization. A larger number M increases CPU-time and storage requirements. A smaller number increases the likelihood of having one or less SRD-particles per bin so that no collisions take place; yielding a much larger *effective* mean free path (see below) and poor resolution of the flow field.

At constant time step, temperature and fluid density $\rho_f = Mm_f/a_0^3$, leads to a smaller m_f and a larger effective mean free path (cf. eqs. below) of the fluid particles, which leads to a bad resolution of the flow field around the particle. We note that the dependence of the transport coefficients on this number density is weak, cf. [3].

Perhaps the most critical parameter is the mean-free path. It is defined as

$$\lambda = \Delta t_{srd} \sqrt{k_b T / m_f}$$

λ represents the average distance traveled between collisions of srd particles, which is clearly set by the SRD time step and the mean-thermal speed $(k_b T/m_f)^{1/2}$. Here k_b is the Boltzmann constant. In order to maintain Galilean invariance λ must be greater than $0.5a_0$, for our implementation [21].

In summary, if the bin size is set according to the colloid size at $a_0 = R/2$ and the average number of srds per bin is in the target range of 3 to 6, LAMMPS needs three quantities for closure: m_f, Δt_{srd}, and $k_b T$. We need to choose these so that $\lambda > 0.5a_0$, and so that we best reproduce all of the key dimensionless quantities, viz. the Peclet number, Pe (ratio of a convective time scale to a diffusion time scale) and the particle Reynolds number, *Re*. One way to do so is to choose the parameters to get as close as possible to the diffusion coefficient given by the Stokes-Einstein relation. The Stokes-Einstein relation requires knowledge of the shear viscosity of the solvent. Transport coefficients for various SRD implementations have been derived in reference [21]. The kinematic viscosity as a function of the SRD parameters is:

$$\nu = \frac{a_0^2}{18\Delta t_{srd}}\left(1 - \frac{1-e^{-M}}{M}\right) + \frac{k_b T \Delta t_{srd}}{4 m_f}\frac{M+2}{M-2} = \frac{a_0^2}{18\Delta t_{srd}}\left(1 - \frac{1-e^{-M}}{M}\right) + \frac{\lambda^2}{4\Delta t_{srd}}\frac{M+2}{M-2}$$

With our choice of a_0 and M, and choosing a value for $\lambda > 0.5a_0$, it is clear that selecting a Δt_{srd} determines the kinematic viscosity of the SRD fluid or visa versa. Note that setting the viscosity to the value of, say, water yields a time step that is too small to be of practical use. This is one example of the collapsing of time scales these methods allow accesses to longtime information. Alternatively, we could make the time step "large" and set the viscosity to that of the real fluid, but this would lead to impractical values of λ. These are the trade-offs inherent in these types of methods.

Following [2], we determine Δt_{srd} by matching the diffusion coefficient of the model system to that of the physical system in order to maintain the same Pe between the two. Using the Stokes-Einstein equation, $D=k_bT/6\pi\nu\rho R$, and substituting the equation above for ν, noting $k_bT = m_f(\lambda/\Delta t_{srd})^2$, setting the density of the model SRD fluid to that of the real fluid (i.e., $m_f = \rho a_0^3/M$), setting $\lambda = 0.6a_0$, and rearranging we get the following expression for the time step:

$$\Delta t_{srd} = \frac{0.003125R^2}{D_{col}}$$

In this particular approach we have chosen to replicate the actual diffusivity of the colloid. Now it is possible to match the Peclet number of the target system, albeit when the values of λ, Δt_{srd}, and m_f are used to calculate the temperature we find again a mismatch between the model system value the physical system value. This has further consequences for the colloid-colloid interaction potentials. We want the keep the ratio of the kinetic energy and the potential energy in the model system equivalent to that in the real system so we will need to scale the colloid-colloid interaction parameters accordingly. Nonetheless we have achieved dynamic similarity with respect to the balance of thermal motion and convection.

Matching conditions and parameters of a real system of nanoparticles in solvent is difficult with coarse-grained techniques like SRD. To reach this goal we first pursued verification of several fundamental problems known in the literature followed by validation against a real system of nanoparticles in solvent. Towards this end, we report here sample results in the following cases:

-Couette flow of pure SRD solvent system

-Diffusion of hard sphere-like nano-colloids in SRD solvent, as a function of nano-colloid concentration

-Shear flow of hard sphere-like nano-colloid suspension (bulk viscosity as a function of colloid concentration)

-Shear flow of a suspension of silica particles in solvent (comparing model system to physical)

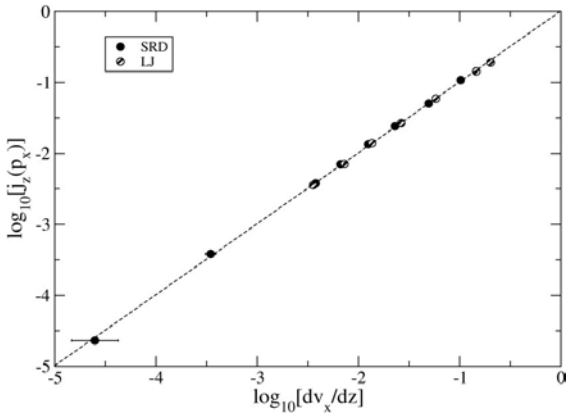

FIGURE 5: Total momentum flux vs. shear rate in pure SRD solvent flow. Flow is Couette (or simple shear) generated by the Müller-Plathe [22] algorithm.

In Fig. 5 we show verification results for a pure-solvent system, viz. a system with only SRD particles. Here we simulate a simple Couette flow with a shear stress applied at opposing boundaries of a three-dimensional box using the Müller-Plathe algorithm [22]. We should point out that the implementation of the Müller-Plathe [22] algorithm for determining the shear viscosity of a mixture of colloid and SRD particles is a unique extension of this work and convenient way to shear a system. Shear stresses on the system are accomplished by simply swapping momentum of particles within thin layers at the top and the middle of the domain in such a way as to conserve momentum. The frequency of swap can be used to adjust the shear rate. The results show that we can achieve a smooth velocity profile statistically. To be accurate, it is desirable that the measured momentum flux be a linear function of shear rate, as would be expected from a Newtonian fluid. Cleary this is the case, as Figure 5 shows.

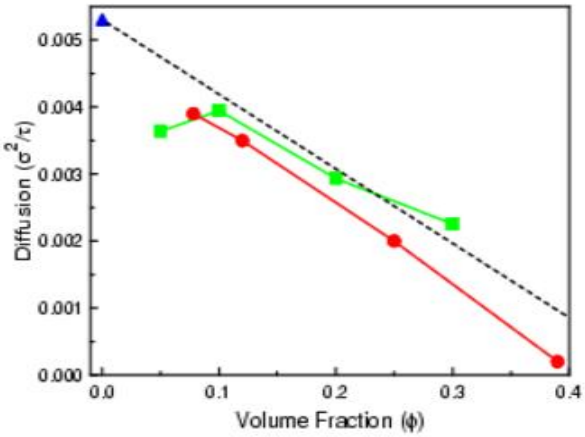

FIGURE 6: Diffusivity versus volume fraction colloid for SRD/colloid simulations (red circles), explicit LJ solvent/colloid (green squares), Stokes-Einstein relation (blue triangle), and the theory of Cichocki and Felderhof [23].

If Fig. 6 we show predicted colloid-diffusion, measured through the mean-square-displacement, at various colloid concentrations. Simulations were performed with SRD/Colloid algorithm and Lennard-Jones particle solvent with larger colloids, both of which are available in LAMMPS. In all cases we have several hundred colloid particles mixed with millions of SRD or LJ solvent

particles. Simulation parameters in both are chosen to give a reduced density $\rho^*=0.6$, dimensionless temperature, or $K_bT/\varepsilon = 1.0$, and dimensionless solvent viscosity $\eta^*=1.0$ (see LAMMPS manual for LJ-unit definitions). In the figure we plot the diffusion predicted with LJ solvent (red), SRD solvent (green), and that predicted with the Stokes-Einstein relation in blue. The reference line (dotted) is predicted from a simplified theory by Cichocki and Felderhof [23]. Clearly all simulations are approaching the limit of Stokes-Einstein theory as the volume fraction approaches zero, and to the theoretical, linear limit of $D_0(1-c\phi)$, with ϕ being the volume fraction. The difference in the LJ and SRD predictions is due to different sized colloids and different colloid-colloid interaction parameters in the two simulations. We are currently performing simulation with identical colloid parameters.

While producing these results we characterized the performance of the coupled colloid-SRD algorithm in LAMMPS. The simulations at one particular concentration were run with the SRD algorithm with the required number of SRD particles per lattice bin (between 4 and 6) and with 21000 LJ particles per colloid, required to achieve an equivalent density, temperature and viscosity. The SRD simulations took 6.3e-3 CPU seconds per colloid per time step on two CPUs on a Linux Desktop workstation. The same simulation using LJ particles for the solvent took 4.0e-3 CPU seconds per colloid per time step on 125 processors of roughly equivalent processor chip speed. We concluded about a 400-fold speed-up to perform the simulations with the equivalent colloid system size. Moreover, we found that the SRD algorithm scales efficiently in parallel, with a 75% efficiency achieved for this system up to 512 processors.

Satisfied with the results for colloid diffusion in a system that is effectively zero Peclet number, we proceeded to verify our implementation under shearing. The idea is to predict the effective shear viscosity of a suspension of nanoparticles at a specified shear rate and volume fraction. In Fig. 7 we show the shear viscosity as predicted by the Müller-Plathe algorithm versus volume fraction of nanoparticles.

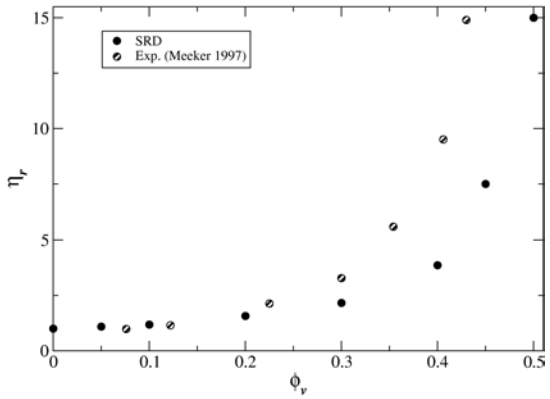

FIGURE 7: Predicted reduced shear viscosity as a function of volume fraction for nanoparticles of diameter $d=20\sigma$. Comparison is shown between SRD and the experimental results of Meeker et al. for hard sphere colloids [43].

Our ultimate goal is to map the SRD parameters to a real nanoparticle-solvent system. At the time of this writing we had not achieved a quantitative agreement with the rheology of a real system. Our current effort is focused on a polystyrene and water system, as it is a common system with numerous data reported in the literature. Specifically, we are simulating the shear-induced flow of a suspension of 390 nm diameter polystyrene particles in water at room

temperature. The nanoparticles hold a charge of 33 mV and an electrolyte is added so that the effective screening length is 4.4 nm. Using this data we prescribed a DLVO pair-wise potential in LAMMPS by deploying a coupled van der Waals and Yukawa hybrid scheme. Simulations were performed using the Müller-Plathe shearing algorithm with a momentum swap rate resulting in shear rates between 10 and 100 s^{-1}. A representative snap-shot of the flow and the resulting average velocity profile are shown in Fig. 8, at a volume fraction of 35% and shear rate of 100 s^{-1}. With this profile, and the accumulated momentum flux in the run we compute an effective viscosity of 3.3e-5 Pa-s. Adjusting this value for the scaling changes needed to match the Pe number, we determine the predicted viscosity at this set of parameters is approximately 0.01 Pa-s, which is of the order of the published experimental data.

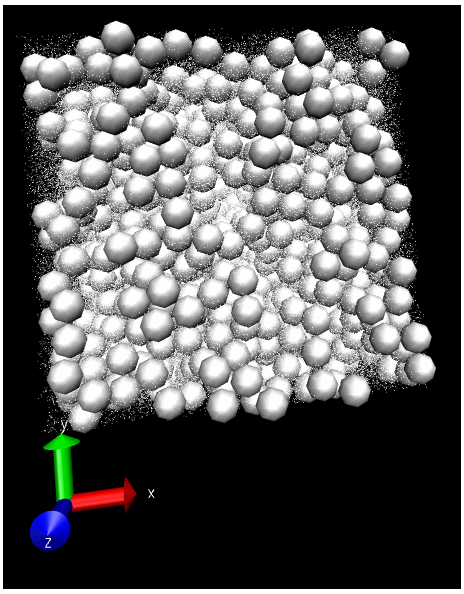

FIGURE 8: Snapshot of simulation of polystyrene in water. Surface potential is 33 mV. Shear rate is 20 s^{-1}.

Nanoparticles in an Explicit Solvent

For weakly interacting colloidal particles, the suspension is well described as a system of hard spheres, while increasing the interaction gives rise to colloidal gels and glasses. Since the size of the colloidal particle is much larger than the solvent, there is a clear separation of time and length scales between the dynamics of the colloidal particles and that of the solvent. This allows one to coarse grain the solvent and treat it as a continuum. However as the size of the colloidal particles are reduced to the low-end of the range of what is now commonly referred to as nanoparticles, e.g. 2-20 nm, treating the background implicitly is not adequate. For example, treating the solvent as a continuum does not account for local packing of the solvent around a nanoparticle which can increase its effective radius. This can modify the effective interactions between nanoparticles, strongly affecting both the structure and dynamics of the suspension. To address even such simple questions as to how large should the nanoparticles be to treat the solvent as a continuum or how do changes in the relative interactions between nanoparticles and between nanoparticles and the solvent affect the suspension rheology, it is important to develop a computationally tractable model of nanoparticle suspensions in which the solvent is treated explicitly.

Most models of colloidal particles treat them as hard spheres. However this approach is not suitable for modeling colloids in an explicit solvent since hard spheres strongly phase separate even for relatively small differences in size [24]. Most simulations of hard spheres have treated the solvent implicitly, usually by Brownian dynamics [25-27]. Stokesian Dynamics [28] and related methods [29] are approaches to include hydrodynamic interactions for the case of implicit solvent. The particle based methods, such as those discussed in Sec. II, introduce an effective coarse-graining length scale that is smaller than the colloids but much larger than the natural length scales of a microscopic solvent.

To solvate the nanoparticles in an explicit solvent, it is critical to include an attractive component of the interaction between the nanoparticle and the solvent. The simplest effective potential is a Lennard-Jones (LJ) interaction shifted to the surface of the nanoparticle [30-33]. However this potential does not capture the true interaction between nanoparticles as the range for which the interactions are important becomes increasingly small with increasing particle size. A more realistic approach is to treat each nanoparticle as being made of a uniform distribution of atoms, similar to treating them as a collection of atoms. For a uniform distribution of atoms, the effective potential can usually be determined analytically [34, 35]. Integrated potentials are computational efficient, although the ability to freely choose shapes is traded for use of symmetrical shapes such as ellipsoids or spheres.

Here nanoparticles are assumed to consist of a uniform distribution of particles interacting with a Lennard-Jones interaction

$$U_{\mathrm{LJ}}(r) = 4\varepsilon_{\mathrm{nn}}\left[\left(\frac{\sigma_{\mathrm{n}}}{r}\right)^{12} - \left(\frac{\sigma_{\mathrm{n}}}{r}\right)^{6}\right],$$

where r is the distance between two atoms. ε_{nn} is the interaction energy and σ_n is the diameter of the LJ atoms which make up each nanoparticle. For spherical nanoparticles, the total interaction between nanoparticles can then be determined analytically by integrating over all the interacting LJ atoms within the two particles [34]. The total interaction between spherical nanoparticles $U_{nn}(r)= U^{A}_{nn}(r)+ U^{R}_{nn}(r)$. $U^{A}_{nn}(r)$ is the standard attractive interaction between colloidal particles, first derived by Hamaker [36]. For particles of equal radii a,

$$U^{\mathrm{A}}_{\mathrm{nn}}(r) = -\frac{A_{\mathrm{nn}}}{6}\left[\frac{2a^2}{r^2-4a^2} + \frac{2a^2}{r^2} + \ln\left(\frac{r^2-4a^2}{r^2}\right)\right].$$

The Hamaker constant $A_{nn} =4\pi^2\varepsilon_{nn}\rho_1\rho_2\sigma_n^6$, where ρ_1 and ρ_2 are the number density of LJ atoms within each sphere. The repulsive component of the interaction $U^{R}_{nn}(r)$ is [34]

$$U^{\mathrm{R}}_{\mathrm{nn}}(r) = \frac{A_{\mathrm{nn}}}{37800}\frac{\sigma_{\mathrm{n}}^6}{r}\left[\frac{r^2-14ra+54a^2}{(r-2a)^7} + \frac{r^2+14ra+54a^2}{(r+2a)^7} - 2\frac{(r^2-30a^2)}{r^7}\right],$$

These last two equations reduce to the standard LJ potential in the limit $a \to 0$ and $4\pi a^3\rho_i/3 = 1$. The total interaction potential between nanoparticles is shown in Fig. 9 for several values of the nanoparticle radii a.

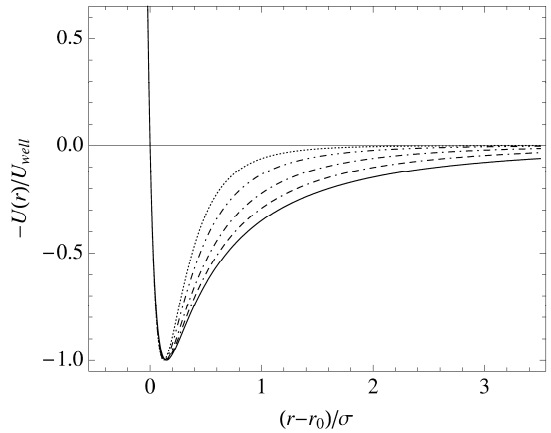

FIGURE 9: Integrated nanoparticle/nanoparticle potential for Lennard-Jones potential (dashed) and nanoparticles of radii a = 2.5, 5.0, 10.0 and 20.0σ.

The interaction $U_{ns}(r)$ between the LJ solvent atoms and the nanoparticle is determined by integrating the interaction between a LJ solvent atom and the LJ atoms within the particle,

$$U_{ns}(r) = \frac{2\,a^3\,\sigma_{ns}^3\,A_{ns}}{9\,(a^2-r^2)^3}\left[1- \frac{(5\,a^6+15\,a^4\,r^2+63\,a^2\,r^4+15\,r^6)\,\sigma_{ns}^6}{15\,(a-r)^6\,(a+r)^6}\right],$$

where $A_{ns} = 24\pi\varepsilon_{ns}\rho_1\sigma_{ns}^3$. Here ε_{ns} is the interaction between a solvent atom and an atom in the nanoparticle and $\sigma_{ns} =(\sigma_n + \sigma_s)/2$, where σ_s is the size of a LJ solvent atom. The interaction between solvent atoms is the same Lennard-Jones interaction given above with $\varepsilon_{ss} = \varepsilon$ and $\sigma_s = \sigma$. Note that, unlike most interaction potentials, $U_{nn}(r)$ and $U_{ns}(r)$ depend on both the size of the atoms making up the nanoparticle σ_n and the radii of the nanoparticle a.

Depending on the values of the Hamaker constant, the nanoparticles can either be dispersed in the solvent or aggregate. For nanoparticles made of the same Lennard-Jones atoms as the solvent ($\varepsilon_{nn} = \varepsilon_{ns} = \varepsilon$ and $\sigma_n = \sigma$), the nanoparticles and solvent phase separate for any value of the density ρ_1 which make up the nanoparticles. To solvate the nanoparticles, the interaction strength ε_{ns} has to be increased relative to ε_{nn}. For $\varepsilon_{nn} = \varepsilon$, simulations were run for several values of ε_{ns}. We found that increasing $\varepsilon_{ns}=3\varepsilon$ was not sufficient to avoid phase separation, while $\varepsilon_{ns}=6\varepsilon$ was. Since increasing the interactions between nanoparticles and solvent further gave an unphysical situation in which a layer or two of solvent atoms were attached to each nanoparticle, we chose to run all the simulations with $\varepsilon_{ns}=6\varepsilon$.

In this study we chose three values for the nanoparticle/nanoparticle interaction strength. For the first, we considered that each nanoparticle was made of a LJ solid which has a density $\rho_1\sigma^3 =1.0$. This gives $A_{nn} = 4\pi^2\varepsilon$. This corresponds to a very strong interaction between the nanoparticles, resulting in a colloidal gel [37]. For nanoparticles of the same density as the solvent, $\rho_1\sigma^3 =0.57$,

the Hamaker constant is reduced significantly, $A_{nn} = 12.9\varepsilon$. However in most nanoparticle suspensions, the nanoparticles are coated with short surfactants to avoid flocculation. Using the present form of the potential, this can be modeled by reducing Ann further. In fact by varying the Hamaker constants it is possible to control the relative strength of the nanoparticle/nanoparticle and nanoparticle/solvent interaction. $A_{nn} = \varepsilon$ as we show below, describes a hard sphere-like nanoparticle suspension for $a = 5\sigma$. In this report, we study how the structure and viscosity of the nanoparticle suspensions depend on the Hamaker constants A_{nn} and A_{ns} for $a = 5\sigma$. Results for $a=10\sigma$ can be found in ref. 37.

All molecular dynamics simulations were performed using the LAMMPS simulation package [5]. As part of this project a number of improvements to the algorithm were made to improve the speed for particles of disparate size. These are described in a recently published paper by in 't Veld *et al.* [6] and include multi-region neighbor lists and enhanced communications, have made the simulations presented here possible. For example the speed up over previous versions of the code for nanoparticles of radii $a = 10\sigma$ in an explicit solvent of LJ atoms is 200-400 times depending on nanoparticle concentration. These enhancements are available at http://lammps.sandia.gov.

Each configuration is prepared by combining a nanoparticle suspension in an implicit solvent with an equilibrated pure solvent of Lennard-Jones particles. The pure solvent and nanoparticle suspension are merged by removing any solvent monomers that overlap a nanoparticle. This configuration is then equilibrated in an NPT ensemble at a temperature $T = \varepsilon/k_B$ and $P = 0.1\varepsilon/\sigma^3$ to ensure a homogenous suspension. All results presented here are for an NVT ensemble. To reduce the number of parameters we set $\sigma_n = \sigma_s = \sigma$ and mass $m_p = 4/3\ \pi\ a^3\rho_1 m$ with $\rho_1\sigma^3 = 1.0$ throughout. Here m is the mass of the solvent monomer.

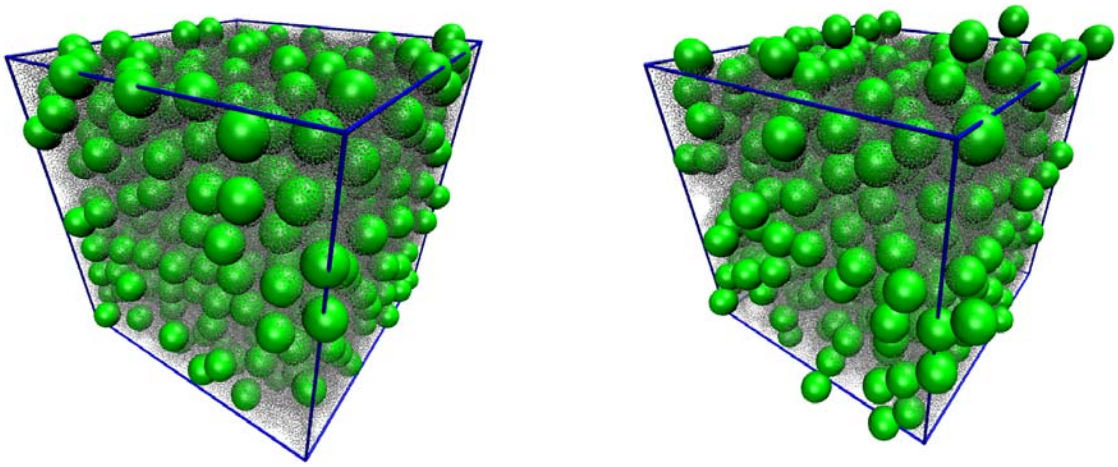

FIGURE 10: Sample simulation cell for N nanoparticles of radii $a = 5\sigma$ for $\phi_v = 0.25$ in an explicit solvent for (a) monomers and (b) dimers. Solvent is shown as points.

For equilibrium simulations Newton's equations of motion were integrated using a velocity-Verlet algorithm coupled weakly to a heat bath [26] with a damping constant $\Gamma = 0.01\tau^{-1}$. The integration time step $\delta t = 0.005\tau$, where $\tau = \sigma(m/\varepsilon)^{1/2}$. The interactions between LJ atoms were

cutoff at r_c =3.0σ, between nanoparticles at 5a and between LJ solvent atoms and nanoparticles at a = 4.0σ. The number of nanoparticles varied from N_n = 10 to 750 and LJ solvent atoms from a few thousand to six hundred thousand depending on the volume fraction $\phi_v = 4N_n/3\ \pi a^3/V$ of nanoparticles. Note this definition of ϕ_v slightly underestimates the volume fraction since $U_{nn}(r)$ =0 for r = 10.44σ > 2a for a=5σ unlike the case of two LJ monomers where $U_{LJ}(r) = 0$ for r = σ. However since the separation r where $U_{nn}(r) = 0$ depends on the nanoparticle radii a, this is a convenient definition. For the dimer system, pairs of nanoparticles are constrained to have a fixed bond length b_n = σ using the SHAKE algorithm. Sample configurations for a monomer and dimer system for a = 5σ and ϕ_v =0.25 are shown in Fig. 10. To determine the shear viscosity, the nanoparticle suspensions were sheared with the SLLOD equations of motion [39-42].

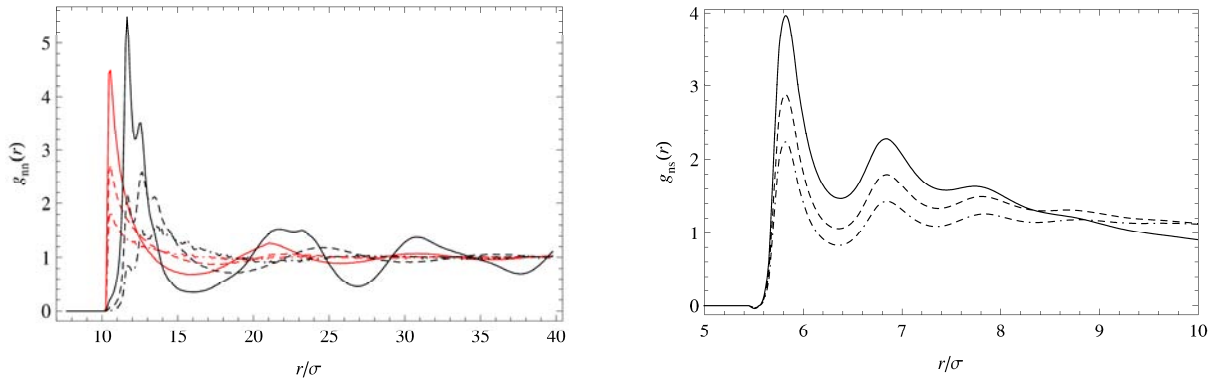

(a) (b)

FIGURE 11: (a) Nanoparticle-nanoparticle pair correlation functions $g_{nn}(r)$ and (b) nanoparticle/solvent pair correlation function $g_{ns}(r)$ for nanoparticles of radii a = 5σ for volume fractions ϕ_v =0.12 (dot-dashed), 0.25 (dashed) and 0.39 (solid) for A_{nn} = ε, A_{ns} = 72ε with explicit solvent (black) and implicit solvent (red).

The effect of including the solvent on the nanoparticle/nanoparticle pair correlations function $g_{nn}(r)$ is shown in Fig. 11a for the hard sphere-like nanoparticles for an explicit and implicit solvent. The simulations for the latter are the same as in the case of the explicit solvent except that the solvent is removed. Note that the first peak in g(r) is higher for the explicit solvent and shifted to larger separations than for an implicit solvent. The solvent forms a layer near the nanoparticles, so that two nanoparticles cannot approach as closely as in the case of an implicit solvent, resulting in an effective nanoparticle radius which is greater than a. In Fig. 11b the nanoparticle/solvent pair correlation function is shown. Increasing Hamaker constants increases the correlations between nanoparticles and with the solvent. For the strongest interaction case Ann = $4\pi^2\varepsilon$, a layer of solvent particles are essentially bound to each nanoparticle resulting in an almost zero probably that two nanoparticles are ever closer than ~ 12.2σ. From visual observation of the configurations, these systems form a colloid gel with a non-uniform distribution of nanoparticles.

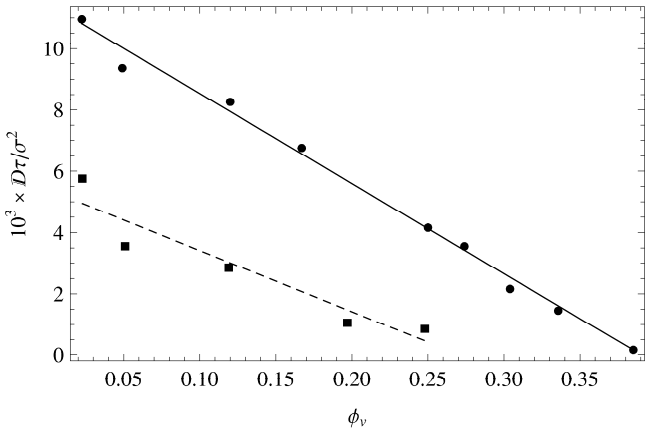

FIGURE 12: Diffusion constant D versus volume fractions ϕ_v for radii a =5ε for $A_{nn} = \varepsilon$, $A_{ns} = 72\varepsilon$ (circles) and $A_{nn} = 12.9\varepsilon$, $A_{ns} = 258\varepsilon$ (squares).

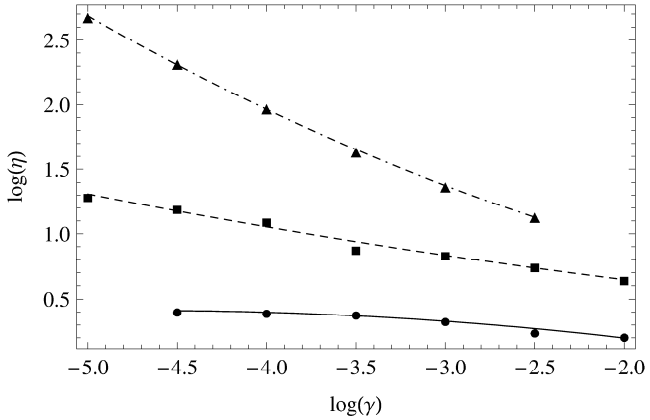

FIGURE 13: Viscosity as a function of shear rate for volume fractions ϕ_v =0.25 for radii a =5σ for $A_{nn} = \varepsilon$, $A_{ns} = 72\varepsilon$ (circles), $A_{nn} = 12.9\varepsilon$, $A_{ns} = 258\varepsilon$ (squares) and $A_{nn} = 4\pi^2\varepsilon$, $A_{ns} = 450\varepsilon$ (triangles).

The effect of varying the Hamaker constant on the diffusion constant D of the nanoparticles is shown in Fig. 12. The result for D at low concentrations is in agreement with the no slip Stokes-Einstein result $D = k_BT/(6\pi\eta_s a) = 0.0105\sigma^2/\tau$, where $\eta_s = 1.01\pm0.02 m/\tau\sigma$ is the viscosity of the pure solvent. The effect of varying the Hamaker constants on the shear rheology is shown in Fig. 13. Clearly increasing the interactions between nanoparticles results in enhanced viscosity as expected. For the strongest interacting case the suspension is in the shear thinning regime for all accessible shear rates. For $Ann = 4\pi^2\varepsilon$, at least in the shear thinning regime which we can presently explore, the viscosity is only weakly dependent on the size of the nanoparticles even for nanoparticles of radii a = 2.5, 5.0 and 10.0σ.

In Fig. 14 we present results for a range of concentrations for hard sphere-like monomers and dimers. Above $\phi_v \sim 0.39$ the monomer nanoparticle suspension crystallizes while the dimers do not over the entire concentration range studied. The liquid/solid transition point is slightly lower than for hard spheres ($\phi_v = 0.494$). This is partially due to the fact that there is a weak interaction between the nanoparticles and underestimation of the volume fraction (radius). For the highest concentrations for the dimers there is some evidence for a shear thickening regime. For $\phi_v \sim$

0.34, the viscosity reaches a plateau at low shear rates and we can extract the zero shear rate viscosity, which is shown in Fig. 15 along with experimental results for hard sphere colloids [43]. These results were fit by the expressions of Krieger and Dougherty [44], $\eta/\eta_s = (1 - \phi_v/\phi_c)^{-2.5\phi c}$ and Quemada [45], $\eta/\eta_s = (1 - \phi_v/\phi_c)^{-2}$. For hard sphere colloids, ϕ_c is typically taken to be between 0.57 and 0.63, the hard sphere glass transition and dense random packing fraction respectively. Fitting the zero shear rate data to the Krieger Dougherty expression gives $\phi_c = 0.39$, whereas the Quemada expression yields $\phi_c = 0.43$. Clearly the fits severely underestimate ϕ_c. As mentioned above, since the nanoparticle-nanoparticle potential is nonzero at the defined nanoparticle radius, ϕ_v slightly underestimates the volume fraction. Also as seen in Fig. 11 there is a weak solvation shell around the nanoparticles limiting the how close the nanoparticles approach each other, increasing the effective volume fraction especially for low ϕ_v. Adjusting the effective radii of the nanoparticle using the onset of the first peak in the nanoparticle pair correlation function, the best fit for $\phi_c = 0.49$ and 0.53 for the Krieger-Dougherty and Quemada expressions respectively.

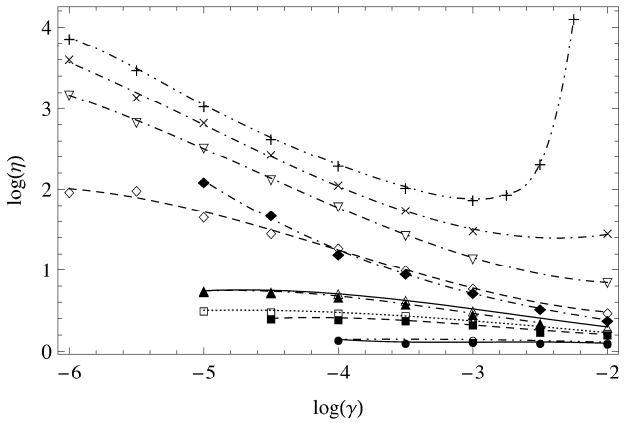

FIGURE 14: Viscosity as a function of shear rate for monomers ($\phi_v \leq 0.39$) (closed) and dimers (open) for $A_{nn} = \varepsilon$, $A_{ns} = 72\varepsilon$ for $\phi_v = 0.12$ (circle), 0.25 (square), 0.31 (triangle), 0.39 (diamond), 0.49 (inverted triangle), 0.54 (cross), and 0.56 (plus).

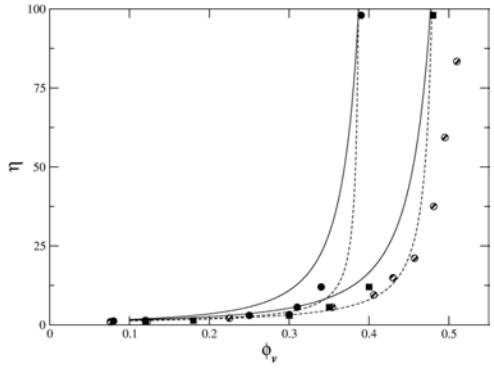

FIGURE 15: Viscosity as a function of ϕ_v for dimers. The circles represent points assuming radii of $a = 5\sigma$ in determining ϕ_v, whereas the squares denote the effective volume fraction for radii adjusted to the peak onset in the nanoparticle pair distribution function. The lines represent the best fit for the Quemada (solid) and Krieger-Dougherty (dashed) expressions for each data set. Also shown are the experimental results for hard sphere colloids [43] (half filled circles).

The effective interaction between spherical nanoparticles given above have been generalized by Everaers and Ejtehadi [34] to model ellipsoidal particles. This potential has been included into LAMMPS. A snapshot of an ellipsoidal nanoparticles in an explicit solvent at ϕ_v =0.20 is shown in Fig. 16. Simulations of the shear rheology for ellipsoids are underway.

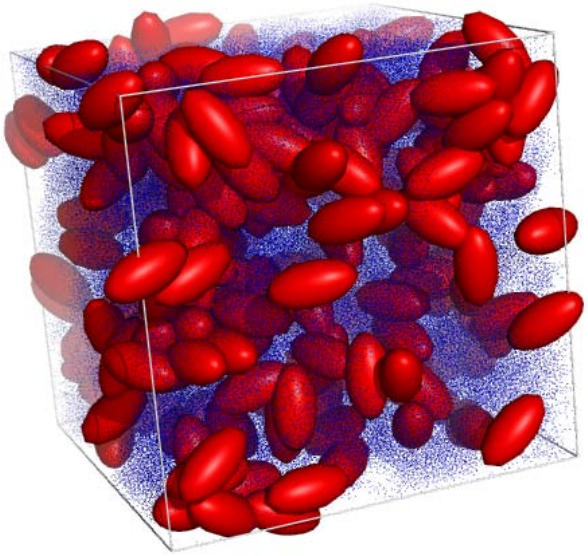

FIGURE 16: Snapshot of ellipsoidal nanoparticles (red) at 20% volume fraction in solvent (blue).

Conclusions

To improve our understanding of the rheology of nanoparticle suspensions we have developed and implemented two "coarse-grained" numerical techniques to provide for high-fidelity numerical simulations of the response and dispersion characteristics typical in a processing flow. The first is a coupled Navier-Stokes/discrete element method in which the background solvent is treated by finite element methods. The second is a particle based method known as stochastic rotational dynamics. Together these two methods provide a new capability representing a "bridge" between the molecular scale and the engineering scale, allowing the study of fluid-nanoparticle systems over a wide range of length and timescales as well as particle concentrations.

To establish the necessary "subgrid" physics for accurate prediction at a larger scale and refining the Navier-Stokes/discrete element and stochastic rotational dynamics methodologies, large scale molecular dynamics simulations have been carried out in which the solvent is included explicitly. Two levels of simulations have been performed. The first is explicit atom simulations to determine the force between nanoparticles as a function of separation. These effective forces are critical input for both of the continuum approaches. The second addresses the question of what is the minimum size of a nanoparticle and bulk concentration of particles at which the continuum fluid-solver approach is valid. From the results shown in Sec. III there are clear effects on the packing and rheology of nanoparticles of size ten times that of the solvent. Using the improvements in the LAMMPS code funded by this project, these studies are presently being extended to nanoparticles of size 20-30 times that of the solvent.

The new capability developed under this LDRD can be used as a technical basis for designing manufacturing processes of nanocomposite materials. Fully-exposed particle/solvent/wall dynamic models can now be interrogated for many of the mechanisms that prevent/allow successful processing. This modeling/simulation capability should be able to support process design within 2-5 years. This work has led to an industrial partnership (CRADA) to develop production-level computational capability aimed at designing nanoparticle flow processing strategies. It is also synergistic with the National Institute for NanoEngineering (NINE) and Center for Integrated Nanotechnology (CINT) in modeling suspensions of aspherical nanoparticles and self-assembly.

References:

[1] W. B. Russel, D. A. Saville, and W. R. Schowalter, Colloidal Dispersions, Cambridge University Press, Cambridge, 1st edition, 1989.
[2] M. Hecht, J. Harting, T. Ihle, and H. J. Herrmann, Phys. Rev. E 72, 011408 (2005).
[3] J. T. Padding and A. A. Louis, Phys. Rev. E 74, 031402 (2006).
[4] A. Malevanets and R. Kapral, J. Chem. Phys. 110, 8605 (1999); J. Chem. Phys. 112, 7260 (2000).
[5] S. Plimpton, J. Comp. Phys. 117, 1 (1995).
[6] P. J. in 't Veld, S. J. Plimpton, and G. S. Grest, Comp. Phys. Comm. 179, 320(2008).
[7] J. H. Irving and J. G. Kirkwood, J. Chem. Phys. 18, 817 (1950).
[8] P. J. Hoogerbrugge and J. M. V. A. Koelman, Europhys. Lett. 199, 155 (1992).
[9] P. Espanol, Phys. Rev. E 57, 2930 (1998).
[10] W. Dzwinel, K. Boryczko, and D. A. Yuen, J. Colloid Interface Sci. 258,163 (2003).
[11] V. Pryamitsyn and V. Ganesan, J. Chem. Phys. 122, 104906 (2005).
[12] R. Codina, J. Comput. Phys. 170, 112 (2001).
[13] D. L. Brown, R. Cortez, M. L. Minion, J. Comput. Phys. 168, 464 (2001).
[14] A. J. C. Ladd, J. Chem. Phys. 88, 5051 (1988).
[15] A. J. C. Ladd and R. Verberg, J. Stat. Phys. 104, 1191 (2001).
[16] G. Gompper, T. Ihle, D. M. Kroll, and R. G. Winkler, Cond. Soft Matter (2008), in press.
[17] Y. Inoue, Y. Chen, H. Ohashi, J. Stat. Phys. 107, 85 (2002).
[18] E. Tüzel, M. Strauss, T. Ihle, and D.M. Kroll, Phys. Rev. E 68, 036701 (2003).
[19] T. Ihle and D. M. Kroll, Phys. Rev. E 67, 066705 (2003).
[20] T. Ihle and D. M. Kroll, Phys. Rev. E 67, 066706 (2003).
[21] T. Ihle and D. M. Kroll Phys. Rev. E 63, 020201 (2001).
[22] F. Müller-Plathe, Phys. Rev. E 59, 4894 (1999).
[23] Cichocki and Felderhof, J. Comp. Phys. 89 (1988).
[24] M. Dijkstra, R. van Roij, and R. Evans, Phys. Rev. E 59, 5744 (1999).
[25] D. L. Ermak and J. A. McCammon, J. Chem. Phys. 69, 1352 (1978).
[26] D. R. Foss and J. F. Brady, J. Fluid Mech. 407, 167 (2000).
[27] D. M. Heyes and H. Sigurgeirsson, J. Rheo. 48, 223 (2004).
[28] J. F. Brady and G. Bossis, Annu. Rev. Fluid Mech. 20, 111 (1988).
[29] R. C. Ball and J. R. Melrose Jr., Adv. Colloid Interface Sci. 59, 19 (1995); A. A. Catherall, J. R. Melrose Jr., and R. C. Ball, J. Rheo. 44, 629 (2000).
[30] M. J. Nuevo, J. J. Morales, and D. M. Heyes, Phys. Rev. E 58, 5845 (1998).
[31] C. Powell, N. Fenwick, F. Bresme, and N. Quirke, Colloids Surf. A 206, 241 (2002).
[32] D. Gersappe, Phys. Rev. Lett. 89, 058301 (2002).
[33] S. R. Challa and F. Van Swol, Phys. Rev. E 73, 016306 (2006).
[34] R. Everaers and M. R. Ejtehadi, Phys. Rev. E 67, 041710 (2003).
[35] T. Desai, P. Keblinski, and S. K. Kumar, J. Chem. Phys. 122, 134910 (2005).
[36] H. C. Hamaker, Physica 4, 1058 (1937).
[37] G. S. Grest, P. J. in 't Veld, and J. B. Lechman, in Complex Systems, Vol. 982, page 304, AIP, 2008.
[38] G. S. Grest and K. Kremer, Phys. Rev. A 33, 3628 (1986).
[39] D. J. Evans and G. P. Morriss, Comp. Phys. Rep. 1, 297 (1984).

[40] J. W. Rudisill and P. T. Cummings, Rheology Acta 30, 33 (1991).
[41] M. E. Tuckerman, C. J. Mundy, S. Balasubramanian, and M. L. Klein, J. Chem. Phys. 106, 5615 (1997).
[42] J. Delhommlle, J. Petravic, and D. J. Evans, Phys. Rev. E 68, 031201 (2003).
[43] S. P. Meeker, W. C. K. Poon, P. N. Pusey, Phys. Rev. E 55, 5718 (1997).
[44] I. M. Krieger and T. Dougherty, Trans. Soc. Rheo. 3, 137 (1959).
[45] D. Quemada, Rheo. Acta 16, 82 (1977).

DISTRIBUTION

1	MS 0899	Technical Library, 9536 (electronic copy)
1	MS 0123	D. Chavez, LDRD Office, 1011 (electronic copy)
1	MS-0382	David Noble, 1514 (electronic copy)
1	MS-0836	Randy Schunk, 1516 (electronic copy)
1	MS-0836	Joel Lash, 1516 (electronic copy)
1	MS-0836	Jeremy Lechman, 1516 (electronic copy)
1	MS-1303	Gary Grest, 1114 (electronic copy)
1	MS-1314	Matt K. Petersen, 1114 (electronic copy)
1	MS-1316	W. Michael Brown, 1416 (electronic copy)
1	MS-1316	Steven Plimpton, 1416 (electronic copy)
1	MS-1411	Nelson Bell, 1816 (electronic copy)
1	MS-1411	David Tallant, 1822 (electronic copy)
1	MS-1411	Amalie Frischknecht, 1814 (electronic copy)
1	MS-1415	Carlos Gutierrez, 1114 (electronic copy)


Sandia National Laboratories